Cellular and Subcellular Heterogeneity of $[Ca^{2+}]_i$ in Single Heart Cells Revealed by Fura-2

W. G. WIER, M. B. CANNELL,* J. R. BERLIN, E. MARBAN, W. J. LEDERER

Digital imaging of calcium indicator signals (fura-2 fluorescence) from single cardiac cells has revealed different subcellular patterns of cytoplasmic calcium ion concentration ($[Ca^{2+}]_i$) that are associated with different types of cellular appearance and behavior. In any population of enzymatically isolated rat heart cells, there are (i) mechanically quiescent cells in which $[Ca^{2+}]_i$ is spatially uniform, constant over time, and relatively low; (ii) spontaneously contracting cells, which have an increased $[Ca^{2+}]_i$, but in which the spatial uniformity of $[Ca^{2+}]_i$ is interrupted periodically by spontaneous propagating waves of high $[Ca^{2+}]_i$; and (iii) cells that are hypercontracted (rounded up) and that have higher levels of $[Ca^{2+}]_i$ than the other two types. The observed cellular and subcellular heterogeneity of $[Ca^{2+}]_i$ in isolated cells indicates that experiments performed on suspensions of cells should be interpreted with caution. The spontaneous $[Ca^{2+}]_i$ fluctuations previously observed without spatial resolution in multicellular preparations may actually be inhomogeneous at the subcellular level.

QUANTITATIVE MEASUREMENT OF the concentration of intracellular calcium ions ($[Ca^{2+}]_i$) in heart muscle has been made difficult by the lack of information about the spatial distribution of $[Ca^{2+}]_i$ (*1*), by the properties of the previously available calcium indicators (*2*), and by the necessity to use multicellular cardiac preparations [but see (*3*)] or suspensions of cardiac cells. Recently, new calcium indicators have become available which, because of their improved properties (*4*), can be used in single isolated cells (*5*). We report here the first use of one such calcium indicator, fura-2 (*4*), coupled with digital imaging fluorescence microscopy (*6, 7*), to examine the spatial and temporal distribution of calcium within individual, enzymatically dissociated rat heart cells.

Single rat ventricular cells, loaded with fura-2, were studied by means of an inverted microscope equipped with an epifluorescence illuminator, an ultrasensitive video camera, and a photomultiplier tube. The methods were similar to those described in our preliminary reports (*8*) and by Williams *et al.* (*9*). After isolation (*10*), cells were loaded with fura-2 by exposure to the acetoxymethyl ester fura-2 AM, at a concentration of 5 μM, for 15 to 30 minutes. We estimate that the concentration of fura-2 in these cells was 50 to 100 μM; this estimate is based on comparison to cells loaded with 0.2 mM fura-2 (pentapotassium salt) via a patch pipette. A small portion of fura-2–loaded cells was placed in an experimental chamber (*11*), which was mounted on the stage of an inverted microscope. The bathing solution contained 145 mM NaCl, 4 mM KCl, 1 mM $MgCl_2$, 1 mM $CaCl_2$, 10 mM glucose, and 10 mM Hepes (*N*-2-hydroxyethylpiperazine-N′-2-ethanesulfonic acid, *p*H 7.4), and was maintained at 35°C. The cell selected for study could be illuminated by transmitted visible light (Fig. 1A) or by ultraviolet (UV) light, via an epifluorescence illuminator constructed from fused silica optical elements and a 150-W xenon or 100-W mercury arc lamp. Illumination with UV light at a wavelength of 340 nm or 380 nm was selected by 10-nm bandwidth interference filters. Emitted light was filtered at 510 nm and was focused on an ISIT (intensified silicon intensifier target) camera (RCA TC1040/H or Dage 66) and a photomultiplier tube (EMI 9635B or EMI 9698). Four images were recorded for each measurement of $[Ca^{2+}]_i$; one image each of the cell with illumination at 340 nm and 380 nm, and one image each of "background" (after removal of the cell with a micropipette), with illumination at each of the two excitation wavelengths. Background images and a constant value equal to mean autofluorescence were subtracted from the images of the cells. Images of fluorescence ratios (Fig. 1D) were then obtained by dividing, pixel by pixel, the 340-nm image after background subtraction (Fig. 1B) by the 380-nm image after background subtraction (Fig. 1C) (*12*).

The intensity of the fluorescence of the fura-2 is somewhat nonuniform in single quiescent rat cardiac cells (Fig. 1, B and C). However, this spatial variation is correlated with variation in thickness of the cell, as observed in transmitted light images (Fig. 1A), and not usually with any identifiable intracellular organelle or cellular structure. Occasionally, the two nuclei typical of cardiac cells were visible as two localized regions of increased fluorescence. However, the images of fluorescence ratios (Fig. 1D) or "surface plots" of fluorescence ratios (Fig. 2A and lower cell in Fig. 3A) are always quite uniform; patterns of variation in fluorescence intensity sometimes evident in the individual fluorescence images are never evident in the ratios. This suggests that $[Ca^{2+}]_i$ is uniform in these cells under these conditions. Any uncertainty (see below) about the exact calibration curve to use would not affect this conclusion. Furthermore, as

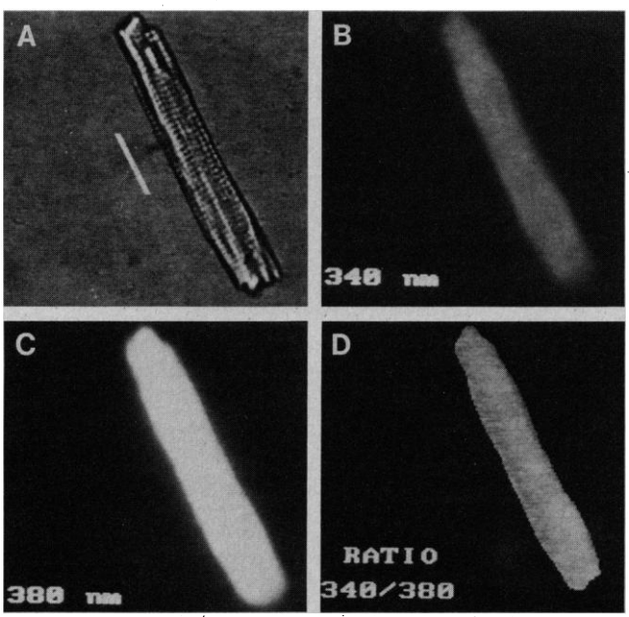

Fig. 1. (**A**) Transmitted-light image of a single rat ventricular cell. The scale bar beside the cell is 20 μm. (**B**) Image of the same cell at 510 nm after background subtraction; the cell was illuminated with light at 340 nm. (**C**) Image of the same cell after background subtraction; the cell was illuminated with light at 380 nm. (**D**) Image of fluorescence ratios in the cell, obtained as described [in the text and (*12*)].

W. G. Wier, M. B. Cannell, J. R. Berlin, W. J. Lederer, Department of Physiology, University of Maryland School of Medicine, Baltimore, MD 21201.
E. Marban, Division of Cardiology, Department of Medicine, The Johns Hopkins University, Baltimore, MD 21205.

*Present address: Department of Pharmacology, University of Miami, School of Medicine, Miami, FL 33101.

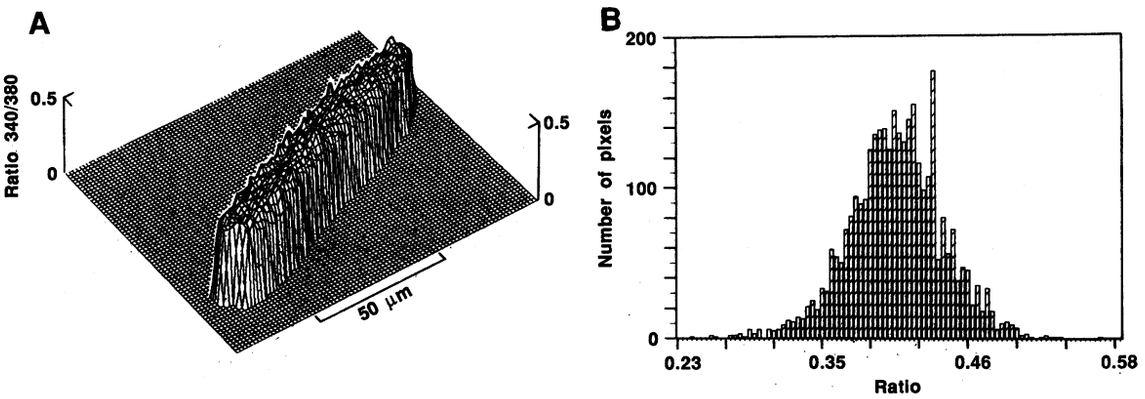

Fig. 2. Analysis of fluorescence ratios of a single cell. (**A**) Surface plot of fluorescence ratios in the cell shown in Fig. 1. The ratio is uniform over the surface of the cell. (**B**) Histogram of fluorescence ratios in the same cell as in Fig. 1. The fluorescence ratio was 0.401 ± 0.040 (SD).

shown in Fig. 2B, the distribution of the values of ratios in an image is narrow; for the cell in Fig. 2, it is approximately Gaussian, with a mean and standard deviation (SD) of 0.401 and 0.040, respectively. Since the fluorescence ratio appears to be uniform across the cell, the spatial information contained within the image can be ignored to enable the standard error of the mean to be calculated. When this is done the precision of the mean ratio becomes very high; for example, the standard error of the mean ratio for the cell depicted in Figs. 1 and 2 is only 0.0007.

For cells that have a spatially uniform $[Ca^{2+}]_i$, the spatially averaged signal provided by a photomultiplier tube can be used to measure the fluorescence ratio. This method not only decreases the amounts of data that have to be stored and simplifies data analysis, but also gives improved temporal resolution when transient changes in $[Ca^{2+}]_i$ occur. In a single cell, repetitive measurements of the fluorescence ratio with this method were associated with little variability; in one quiescent cell, ten successive measurements had a mean and standard deviation of 0.35 and 0.004, respectively. To be certain that the two techniques give the same answer, we measured mean ratios with digital imaging microscopy and with the photomultiplier tube simultaneously in specific cells. There were no systematic differences in the mean ratios calculated with the two methods. The mean ratio in 22 quiescent cells from one rat was 0.55 with an SD of 0.08. The range of fluorescence ratios that was observed was somewhat greater than expected given the precision of our measurement system. This implies that there are genuine variations in the level of $[Ca^{2+}]_i$ from cell to cell, even among quiescent cells, that were not distinguishable on the basis of either behavior or morphology.

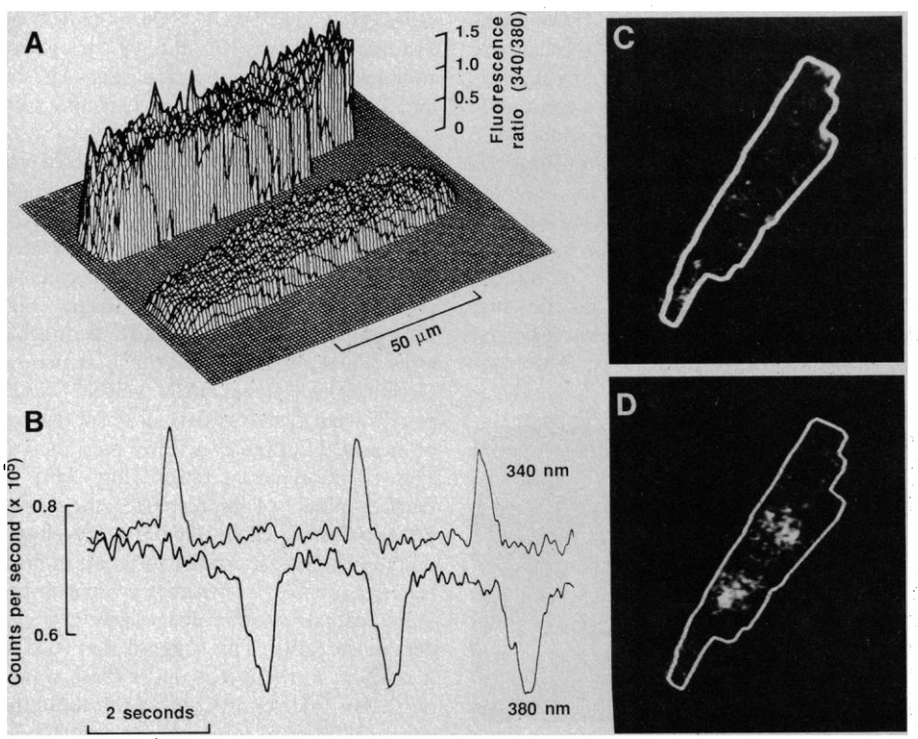

Fig. 3. Spatial and temporal heterogeneity of $[Ca^{2+}]$ in spontaneously active cells. (**A**) Three-dimensional plot of fluorescence ratios in a quiescent cell (lower) and a spontaneously active cell (upper), in the interval between $[Ca^{2+}]_i$ fluctuations. (**B**) Recordings of changes in fluorescence intensity at 340-nm and 380-nm illumination during spontaneous $[Ca^{2+}]_i$ fluctuations or waves in $[Ca^{2+}]_i$. The photomultiplier tube recorded the two signals sequentially. (**C** and **D**) Imaging of spontaneous subcellular inhomogeneity of $[Ca^{2+}]_i$. The image in (C) is the control image for that in (D) and was obtained by subtracting one image from another image, both of which were obtained in the absence of a wave. The image in (D) was obtained by subtracting an image, obtained in the absence of a wave, from an image obtained during a wave. Thus, the increased intensity in the crescent-shaped regions implies increased $[Ca^{2+}]_i$ in those regions. The two crescent-shaped regions near the center of the cell propagated from a region approximately halfway between them. The images in (C) and (D) have been subjected to a low-pass spatial filter to reduce photon noise.

In all experiments, a fraction of the cells exhibited spontaneous contractile activity—either propagating, locally contracting regions or, less frequently, synchronous contractions. The actual fraction of such cells has been shown previously to depend on a number of factors (*13*). Spontaneously active cells were not distinguishable at rest from quiescent cells, and we grouped cells on the basis of whether or not they showed any spontaneous contractile activity within a 1-minute period. In the spontaneously active cells the fluorescence ratio was greater than that in quiescent cells and could be spatially nonuniform. Figure 3A illustrates the difference in fluorescence ratios between a quiescent cell and a spontaneously active cell. The cell with the low ratio was quiescent, whereas the one with the high ratio was spontaneously active at a relatively high frequency and shortened markedly a few minutes after this image was acquired. (The image was acquired in an interval between spontaneous contractions.) The mean fluorescence ratio in six cells that were spontaneously active was 0.85 ± 0.17 (SD), which was significantly different from that in the 22 quiescent cells from the same rat (*t* test, $P < 0.05$). In spontaneously active cells,

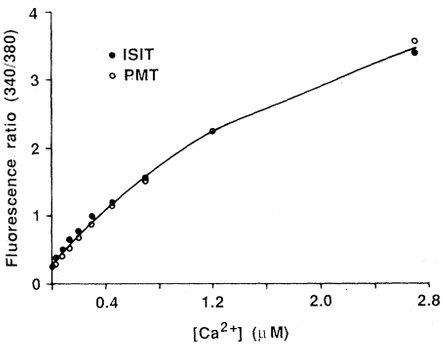

Fig. 4. Calibration curve of fura-2 fluorescence ratio. The relation between $[Ca^{2+}]$ and ratios of fluorescence of fura-2 was determined by illuminating through the microscope, at 340 nm and 380 nm, small volumes of calibrating solution containing 50 μM fura-2 pentapotassium salt and calcium ions at various concentrations. The EGTA-buffered calibrating solutions [*p*H 7.1; 35°C; dissociation constant (K_d) of EGTA, 294 n*M*] used to titrate fura-2 with Ca^{2+} were prepared as previously described (*4*). The fluorescence emission at 510 nm was detected with the photomultiplier tube (PMT) and with the ISIT camera. Images of fluorescence ratios in the calibrating solutions were obtained as described [in the text and in (*12*)]. The mean fluorescence ratio in the image obtained with the ISIT (filled circles) and the ratio obtained with the photomultiplier tube (open circles) are plotted as a function of $[Ca^{2+}]$. The close agreement between the fluorescence ratios obtained with the ISIT data and those obtained with the photomultiplier tube indicates that the processing of the video signal was correct; that is, all nonlinearities had been properly corrected. The K_d of fura-2, calculated by the method of Grynkiewicz *et al.* (*4*) for calcium was 320 n*M*.

one could observe wavelike changes in fluorescence that seemed to accompany the propagating local contractions. The "waves" of fluorescence change, whose propagation velocity was approximately 100 μm/sec, consisted of increased (at 340-nm illumination) or decreased (at 380-nm illumination) fluorescence (Fig. 3B). These propagating waves of fluorescence change were also recorded with the video system, as shown in Fig. 3D (control image in Fig. 3C). The contrast of these images has been enhanced digitally to make clear the spatially localized change in fluorescence. However, at present, the speed of response of the video system and the spontaneous nature of the oscillations precludes precise quantification of fluorescence ratios within these regions. Cells with such relatively high and spatially inhomogeneous $[Ca^{2+}]_i$ may be responsible for the spontaneous $[Ca^{2+}]_i$ fluctuations detected by noise analysis of aequorin light signals in multicellular preparations (*14*). The fluctuations of $[Ca^{2+}]_i$ are also thought to activate certain membrane currents (*15*). Furthermore, the heterogeneity of mechanical activity in populations of isolated heart cells, which we now observe to be correlated with $[Ca^{2+}]_i$, has been shown previously to be correlated with mechanical properties of intact heart muscle (*16*).

The third class of cells that we examined were myocytes that were hypercontracted or "rounded up." The amount of fura-2 contained in 11 such cells (from the same animal as above) was highly variable, as was the fluorescence ratio [1.85 ± 1.2 (SD)]. In such cells the fluorescence could spontaneously oscillate, although waves like those described above were not necessarily evident. Since the fura-2 in these cells was not saturated, such cells still regulate $[Ca^{2+}]_i$, although at a relatively high level.

The calculation of cytoplasmic $[Ca^{2+}]_i$ from the fluorescence ratio, even as observed in a single cell, is problematic. Williams *et al.* (*9*) showed that calibration curves obtained in calibrating solutions are close to those obtained in single amphibian smooth muscle cells in which $[Ca^{2+}]_i$ is controlled with ionomycin. However, our preliminary experiments (*17*) in cardiac cells indicate that the dynamic range of the indicator is somewhat reduced inside cells compared to that of thin solutions of fura-2 observed in the microscope (Fig. 4). Therefore, we have emphasized the fluorescence ratios throughout this report and acknowledge the possibility that the absolute levels of $[Ca^{2+}]_i$ calculated from these ratios may have to be revised when the effect of the intracellular environment on fura-2 becomes known. When the calibration curve (Fig. 4) is applied to the data we obtain the following values of $[Ca^{2+}]_i$ (mean and SD): 134 ± 43 n*M* for 22 quiescent cells, 270 ± 91 n*M* for six spontaneously contracting cells, and 955 ± 800 n*M* for 11 hypercontracted cells.

The inevitable heterogeneity of $[Ca^{2+}]_i$ in a population of isolated cardiac cells (Fig. 3A) makes the quantitative interpretation of experiments performed on suspensions of cells in cuvettes (*18*) questionable. Such measurements will reflect, in a complex and unknown way, the heterogeneity of $[Ca^{2+}]_i$ in cells in different physiological conditions as well as the subcellular heterogeneity (Fig. 3D) that exists in a fraction of the cells at any given time. In contrast, measurements of $[Ca^{2+}]_i$ made with digital imaging of fura-2 fluorescence can be made on single cells whose behavior and response to interventions can be characterized.

REFERENCES AND NOTES

1. M. B. Cannell and D. G. Allen, *Biophys. J.* **45**, 913 (1984); D. T. Yue and W. G. Wier, *ibid.* **48**, 533 (1985).
2. J. R. Blinks, W. G. Wier, P. Hess, F. G. Prendergast, *Prog. Biophys. Mol. Biol.* **40**, 1 (1982).
3. P. H. Cobbold and P. K. Bourne, *Nature (London)* **312**, 444 (1984).
4. G. Grynkiewicz, M. Poenie, R. Y. Tsien, *J. Biol. Chem.* **260**, 3440 (1985).
5. R. Y. Tsien, T. J. Rink, M. Poenie, *Cell Calcium* **6**, 145 (1985); M. Poenie, J. Alderton, R. Y. Tsien, R. A. Steinhardt, *Nature (London)* **315**, 147 (1985); D. A. Williams, R. Y. Tsien, F. S. Fay, *Biophys. J.* **47**, 131a (1985); W. Almers and E. Neher, *ibid.* **49**, 338a (1986).
6. B. Tycko, C. H. Keith, F. R. Maxfield, *J. Cell Biol.* **97**, 1762 (1983); R. D. Allen and N. S. Allen, *J. Microsc.* **129**, 3 (1983).
7. L. Tanasugarn, P. McNeil, G. T. Reynolds, D. L. Taylor, *J. Cell Biol.* **98**, 717 (1984).
8. J. R. Berlin *et al.*, *J. Physiol. (London)* **371**, 200P (1985); W. G. Wier and E. Marban, *Biophys. J.* **49**, 466a (1986); M. B. Cannell, W. G. Wier, J. R. Berlin, E. Marban, W. J. Lederer, *ibid.*, p. 466a.
9. D. A. Williams, K. E. Fogarty, R. Y. Tsien, F. S. Fay, *Nature (London)* **318**, 558 (1985).
10. J. R. Hume and W. R Giles, *J. Gen. Physiol.* **78**, 19 (1981); G. Isenberg and U. Klockner, *Pfluegers Arch.* **395**, 30 (1982).
11. M. B. Cannell and W. J. Lederer, *Pfluegers Arch.* **406**, 536 (1986).
12. Calibration (a linear gray scale), alignment, and timing information were superimposed on the output signal of the camera, which was recorded with a video cassette recorder (Panasonic NV8500). The video signal was viewed, in real time, on a television monitor and oscilloscope. The photomultiplier tube viewed a region of the cell approximately 5 μm in diameter. Output from the photomultiplier tube was recorded simultaneously with the video signal. After processing with a time-base corrector, recorded video signals were digitized (512 × 480 pixels with 256 gray levels). Nonlinearities and image misalignments introduced by the recording equipment were then corrected with use of the calibration information recorded in the video signal. In order to ease storage requirements and to simplify processing, the video frames were then reduced to a resolution of 256 × 240 pixels. "Residual suppression" (*7*) was performed by measuring the standard deviation of pixel values in a small region away from the cells. Unless corresponding pixel values in each frame were at least 10 standard deviations above the background, the pixels were rejected (by the analysis program), and the corresponding pixel in the image of ratios was set to zero. We estimate that the limit of resolution of the system is slightly greater than 1 μm; from a sharply defined cell edge, fluorescence intensity has fallen by half at 1 μm from the cell. Within the cell, however, the spatial resolution would be slightly lower than this because of the photon noise of the image.
13. A. A. Kort, M. C. Capogrossi, E. G. Lakatta, *Circ. Res.* **57**, 844 (1985).
14. C. H. Orchard, D. A. Eisner, D. G. Allen, *Nature (London)* **304**, 735 (1983); W. G. Wier, A. A. Kort, M. D. Stern, E. G. Lakatta, E. Marban, *Proc. Natl. Acad. Sci. U.S.A.* **80**, 7367 (1983).
15. W. J. Lederer and R. W. Tsien, *J. Physiol. (London)* **263**, 73 (1976); R. S. Kass, W. J. Lederer, R. W. Tsien, R. Weingart, *ibid.* **281**, 187 (1978); D. Colquhoun, E. Neher, H. Reuter, C. F. Stevens, *Nature (London)* **294**, 752 (1981); R. S. Kass and R. W. Tsien, *Biophys. J.* **38**, 259 (1982); H. Matsuda, A. Noma, Y. Kurachi, H. Irisawa, *Circ. Res.* **51**, 142 (1982); A. A. Kort and E. G. Lakatta, *ibid.* **54**, 396 (1984); M. B. Cannell and W. J. Lederer, *J. Physiol. (London)* **374**, 201 (1986).
16. M. C. Capogrossi, A. A. Kort, H. A. Spurgeon, B. A. Suarez-Izla, E. G. Lakatta, *Biophys. J.* **45**, 94a (1984).
17. Preliminary attempts to measure the response of fura-2 to $[Ca^{2+}]_i$ inside single cardiac cells have shown R_{max} (the fluorescence ratio obtained when fura-2 is saturated with calcium) to be somewhat less than is measured from the curve of Fig. 1. However, technical difficulties associated with the ionomycin method in single cardiac cells have prevented us from resolving this issue quantitatively. In addition, a small fraction of fura-2 fluorescence is not releasable with digitonin, suggesting that this small fraction may arise from bound or sequestered fura-2 or fura-2 AM (W. G. Wier, S. W. Robinson, L. Barcenas-Ruiz, in preparation).
18. S-S. Sheu, V. K. Sharma, S. P. Banerjee, *Circ. Res.* **55**, 830 (1984); S-S. Sheu, V. K. Sharma, A. Uglesity, *Am. J. Physiol.* **250**, C656 (1986); A. P. Thomas, M. Selak, J. R. Williamson, *J. Mol. Cell. Cardiol.* **18**, 541 (1986); D. Ashen, W. F. Goldman,

T. Ashida, M. P. Blaustein, *Biophys. J.* **49**, 14a (1986).
19. Supported by NIH grants HL29473 (to W.G.W.) and HL25675 (to W.J.L.) and by grants from the American Heart Association and the Maryland Heart Association (to W.G.W., M.B.C., J.R.B., and W.J.L.). W.G.W. and W.J.L. are Established Investigators of the American Heart Association and its Maryland Affiliate. M.B.C. is the Young Investigator of the Maryland Affiliate of the American Heart Association. We thank R. J. Bloch for the use of his Dage 66 ISIT video camera and K. E. MacEachern and V. P. Toney for assistance in preparation of the manuscript.

6 August 1986; accepted 21 November 1986

A Subset of Yeast snRNA's Contains Functional Binding Sites for the Highly Conserved Sm Antigen

NORA RIEDEL, SANDRA WOLIN, CHRISTINE GUTHRIE

Autoimmune sera of the Sm specificity react with the major class of small nuclear RNA (snRNA)–containing ribonucleoprotein particles (snRNP's) from organisms as evolutionarily divergent as insects and dinoflagellates but have been reported not to recognize snRNP's from yeast. The Sm antigen is thought to bind to a conserved snRNA motif that includes the sequence A(U_{3-6})G. The hypothesis was tested that yeast also contains functional analogs of Sm snRNA's, but that the Sm binding site in the RNA is more strictly conserved than the Sm antigenic determinant. After microinjection of labeled yeast snRNA's into *Xenopus* eggs or oocytes, two snRNA's from *Saccharomyces cerevisiae* become strongly immunoprecipitable with human autoantibodies known as anti-Sm. These each contain the sequence A(U_{5-6})G, are essential for viability, and are constituents of the spliceosome. At least six other yeast snRNA's do not become immunoprecipitable and lack this sequence; these non-Sm snRNA's are all dispensable.

SMALL NUCLEAR RNA'S (SNRNA'S) are found complexed with proteins as small nuclear ribonucleoproteins (snRNP's) (*1*). In higher eukaryotes, five of the six most abundant snRNA's (U1, U2, U4–U6) are associated with one or more proteins that react with human autoimmune sera of the Sm specificity (*1, 2*). The functional importance of the Sm snRNP's was predicted by their extraordinary evolutionary conservation: human antisera immunoprecipitate snRNP's from species as divergent as frogs, insects, sea urchins, and dinoflagellates (*3, 4*). Indeed, four of these five U-snRNA's have now been shown to be essential for splicing of messenger RNA precursors (pre-mRNA's) in mammalian cell-free extracts (*5*) and the fifth (U5) is likely to be (*6*).

The evolutionary conservation of the Sm antigen does not seem to extend to lower eukaryotes, however, since the human sera were reported not to immunoprecipitate labeled RNP's from *Dictyostelium* or the yeast *Saccharomyces cerevisiae* (*3*). We have since shown that, like higher eukaryotes, yeast contains nuclear RNA's that possess the trimethylguanosine (TMG) 5′ cap that is specific to snRNA's (*7*). However, the large number of yeast snRNA species (≈24), their low abundance (≈10 to 500 molecules per cell), and their broad size distribution (≈120 to >1000 nucleotides) were unexpected (*7, 8*). Most surprisingly, the first three single-copy *SNR* genes we tested (*SNR3*, *SNR4*, and *SNR10*) were dispensable for growth, a result inconsistent with their participation in essential RNA processing reactions such as splicing (*9–11*).

The Sm antigen is believed to bind to a conserved motif in snRNA's, the sequence A(U_{3-6})G being embedded in a single-stranded region (*12*). The first time we encountered this consensus in a yeast snRNA was in the fourth gene we analyzed, *SNR7* (*13*). *SNR7* was also the first essential snRNA gene we identified (*11*). We thus hypothesized that yeast contains snRNA's that are the functional analogs of the Sm snRNA's, but that the Sm antigenic determinant has diverged too far to be efficiently recognized by human sera. Moreover, we predicted that Sm snRNA's would constitute only a subset of the yeast family and that these species in particular would be required for viability. To test whether snR7 contains a functional Sm binding site and, if so, to identify additional Sm snRNA species, we have taken advantage of observations that *Xenopus laevis* eggs and oocytes contain stockpiles of snRNP proteins and that microinjected snRNA's from HeLa cells or *Drosophila* can assemble with *Xenopus* Sm proteins to become immunoprecipitable with human anti-Sm sera (*14, 15*).

Department of Biochemistry and Biophysics, University of California, San Francisco, CA 94143.

The low abundance of the yeast snRNA's prompted us to choose an enriched source of snR7 for our initial experiments. Fraction I of the yeast splicing extract (*16*), which is generated by ammonium sulfate precipitation, is enriched by a factor of approximately 50 for a subset of RNA's that include snR7 (Fig. 1) (*17*). Fertilized *Xenopus* eggs at the one-cell stage were injected with pCp-labeled fraction I RNA or, as a control, *Drosophila* snRNA's (Fig. 1, lane b). After incubation, extracts were prepared and subjected to immunoprecipitation with anti-Sm antibodies (anti-Sm) (lanes d and m), anti-(U1)RNP antibodies (which is specific for U1 RNA–containing snRNP's) (lanes e and n), or a control nonimmune human serum (lanes f and o). Three RNA species from yeast were efficiently precipitated by anti-Sm (lane d); these are the two forms of snR7 [the longer form, $snR7_l$, contains a 35-nucleotide extension at the 3′ terminus

Table 1. Symbols: ++, quantitative precipitability by anti-Sm; +, strong precipitability; (+) weak (or possibly nonspecific) precipitability; −, no detectable precipitability. Putative Sm sites were identified strictly according to the proposed consensus A(U_{3-6})G (*12*); in the cases of snR7, -14, and -20, the regions containing the consensus sequence are predicted to be single-stranded. According to these criteria of sequence and structure, snR3 would not contain an Sm site and is thus unlikely to be the analog of U4 as we initially suggested (*9*). Disruption phenotype refers to the viability of haploid cells containing null alleles of the test *SNR* gene. These alleles are obtained by performing gene disruptions in vitro. Our typical strategy (*9–11, 23*) is to generate a gene disruption by inserting a second gene with an easily scored phenotype, such as *LEU2*. A linear DNA fragment flanked by sequences homologous to those in the yeast genome is then used to transform diploid cells (in this case, *leu2*−); this one-step gene replacement (*27*) produces cells heterozygous at the *SNR* locus. These diploids are then sporulated. The phenotype (viable or lethal) of spores containing the gene disruption (and therefore *LEU2*) will indicate whether or not the snRNA is essential. Not listed in this table are the other identified snRNA's, for which sequence and gene disruption data are not yet available (*7, 8*).

snR	Anti-Sm ppt	Putative Sm site	Disruption phenotype	Reference
$7_{l,s}$	+	AU_6G	Lethal	(*13*)
14	++	AU_5G	Lethal	(*18*)
17	(+)			
19	(+)			
20		AU_6G, AU_5G, AU_3G	Lethal	(*21*)
3	−	−	Viable	(*9*)
10	−	−	Viable	(*10*)
4	−	−	Viable	(*11, 19*)
5	−	−	Viable	(*19*)
8	−	−	Viable	(*19*)
9	−	−	Viable	(*19*)